

Gamow-Teller  $GT_+$  distributions in nuclei with mass  $A = 90-97$ A. Juodagalvis<sup>1,2</sup> and D. J. Dean<sup>1</sup><sup>1</sup>Physics Division, Oak Ridge National Laboratory, Post Office Box 2008, Oak Ridge, Tennessee 37831-6373, USA<sup>2</sup>Department of Physics and Astronomy, University of Tennessee, Knoxville, Tennessee 37996, USA

(Received 18 June 2004; revised manuscript received 23 March 2005; published 12 August 2005)

We investigate the Gamow-Teller strength distributions in the electron-capture direction in nuclei having mass  $A = 90-97$ , assuming a  $^{88}\text{Sr}$  core and using a realistic interaction that reasonably reproduces nuclear spectroscopy for a wide range of nuclei in the region as well as experimental data on Gamow-Teller strength distributions. We discuss the systematics of the distributions and their centroids. We also predict the strength distributions for several nuclei involving stable isotopes that should be experimentally accessible for one-particle exchange reactions in the near future.

DOI: [10.1103/PhysRevC.72.024306](https://doi.org/10.1103/PhysRevC.72.024306)

PACS number(s): 21.60.Cs, 21.45.+v

## I. INTRODUCTION

New frontiers of nuclear structure experiments to probe the Gamow-Teller distributions in medium-mass nuclei are currently being pursued. These experiments will be able to measure Gamow-Teller data in the mass  $A = 90-100$  region. Extensive theoretical studies have been devoted to Gamow-Teller total strengths and strength distributions in  $1s-0d$  shell nuclei (mass  $A = 16-40$  nuclei) [1] and the  $0f-1p$  shell (mass  $A = 40-80$  nuclei) [2-4]. Because of an excellent agreement between shell-model results and the available experimental data, the calculated results have been used extensively to predict numerous Gamow-Teller strength distributions in nuclei that have not yet become experimentally accessible [5].

In addition to their relevance to nuclear structure, an appropriate description of Gamow-Teller transitions in nuclei directly affects the early phases of type II supernova core collapse since electron capture rates are partly determined by them. The effects of the improved rate estimates are rather dramatic, as was recently discussed in Refs. [6,7]. In addition to the standard Gamow-Teller transitions, first- and second-forbidden transitions contribute to the electron capture rates in the supernova environment. For terrestrial experiments, the primary focus is on the Gamow-Teller transitions.

Recently, Zegers *et al.* [8] proposed measuring the Gamow-Teller distributions using stable Zr and Mo isotopes as targets in ( $t$ ,  $^3\text{He}$ ) reactions [9]. Estimates indicate that the Gamow-Teller strength is sufficiently large to be measured. In this paper, we will investigate these transitions using standard shell-model diagonalization techniques for 36 nuclei in the mass number range  $90 \leq A \leq 97$  ( $Z = 40-47$ ,  $N = 50-57$ ). To validate the interaction, we also studied excitation spectra in those and other nuclei in the region. Since our model space does not contain all spin-orbit partners (i.e., it is not a complete  $0\hbar\omega$  calculation) the total Gamow-Teller strength will be overestimated in our calculations. We adopt a single quenching factor similar to the one discussed in Ref. [10]. We estimated this factor based on recent experimental data on  $^{97}\text{Ag}$  [11]. We used this measurement to gauge our calculation for two reasons. First, it used the total absorption spectrometry, which accounts also for the weak  $\gamma$ -ray cascades that follow

the  $\beta^+$  decay. Second, almost all total Gamow-Teller strength is inside the  $Q$  window. We note that this factor need not be universal as it is simply a phenomenological tool at this point.

The remainder of this paper is organized as follows. In Sec. II, we present results on the nuclear spectra, generated with an effective interaction that uses  $^{88}\text{Sr}$  as a core, and compare them to the experiment. In Sec. III, we present our shell-model diagonalization results for the Gamow-Teller strength distributions and compare these to experimental results when available. We also present systematics of the Gamow-Teller centroids. In Sec. IV, we discuss the distributed-memory shell-model computer code that we developed and used for these calculations. Finally, we conclude and give a perspective in Sec. V.

II. CALCULATED SPECTRA USING THE  $^{88}\text{SR}$  CORE

We perform our shell-model diagonalization calculations in a model space taking  $^{88}\text{Sr}$  as the core nucleus and allowing excitations within the valence space of  $1p_{1/2}$  and  $0g_{9/2}$  proton shells and  $1d_{5/2}$ ,  $2s_{1/2}$ ,  $1d_{3/2}$ ,  $0g_{7/2}$ , and  $0h_{11/2}$  neutron shells. Although our diagonalization cannot be used for calculations of  $\beta$  decays, it appears suitable for Gamow-Teller distributions in the electron-capture direction. The effective interaction [12] was derived from a CD-Bonn potential [13] using the machinery of many-body perturbation theory [14]. We use the following single-particle energies:  $\varepsilon(p_{1/2}) = 0.0$  MeV and  $\varepsilon(g_{9/2}) = 0.9$  MeV for protons; and  $\varepsilon(d_{5/2}) = 0.0$  MeV,  $\varepsilon(s_{1/2}) = 1.26$  MeV,  $\varepsilon(d_{3/2}) = 2.23$  MeV,  $\varepsilon(g_{7/2}) = 2.90$  MeV, and  $\varepsilon(h_{11/2}) = 3.50$  MeV for neutrons. A slightly different version of this interaction was used to describe Sr and Zr isotopes [15]. We have not attempted to adjust the interaction to obtain a better fit to experimental data [16].

We calculated low-energy spectra of more than 50 nuclei with masses in the range  $90 \leq A \leq 98$ , with  $38 \leq Z \leq 48$  and  $50 \leq N \leq 58$ . General agreement between the calculated lowest states and experimentally observed states is satisfactory. We judged the agreement based on reproduction of low-lying states up to a chosen excitation energy. For odd-odd isotopes,

which have a higher density of states, the upper limit was chosen to be 1 MeV. For even-even nuclei the limit was up to 3 MeV. Not all observed states were found in the model space, as would be expected from a restricted calculation, and for some nuclei our calculations suggested some low-lying states that have not yet been observed.

The interaction generally reproduces the correct spin for the lowest states of both parities as well as their ordering, though there are cases where some levels are interchanged. The energy splitting between the lowest states with different parities is reproduced with varying success, although this is difficult to judge for some nuclei because of the lack of experimental information.

For representative spectra that indicate the overall quality of the interaction, we show nuclei having mass  $A = 96$  in Figs. 1 and 2. The maximum energy range shown in the plots is varied following the density of states. From these figures we observe that the spectra of even-even nuclei ( $^{96}\text{Pd}$ ,  $^{96}\text{Ru}$ ,  $^{96}\text{Mo}$ ,  $^{96}\text{Zr}$ , and  $^{96}\text{Sr}$ ) are reproduced well. For  $^{96}\text{Pd}$  there are more calculated states than are experimentally known. In some nuclei the model space is insufficient to describe all observed states. Odd-odd nuclei ( $^{96}\text{Rh}$ ,  $^{96}\text{Tc}$ ,  $^{96}\text{Nb}$ , and  $^{96}\text{Y}$ ), having more states, are also more difficult to describe although, even here, the interaction performs reasonably well. The position of the  $8^+$  isomer in  $^{96}\text{Y}$  is not known experimentally [17]. This state appears in the calculation at a relatively high excitation energy, 1.1 MeV above the lowest positive-parity state, which is calculated to be  $5^+$ . The nucleus  $^{96}\text{Tc}$  reflects a situation where the lowest states are experimentally very close (there are six states in the energy range of 50 keV), whereas the calculation reproduces the states but not their energies (with the calculated range being 310 keV). A similar situation occurs in  $^{92,94}\text{Nb}$ .

These  $A = 96$  nuclei reflect the situation in other cases as well, with a general conclusion that the interaction reproduces excitation spectra reasonably well, though fine-tuning including monopole corrections might increase the accuracy. We do not discuss them in any detail, since the focus of our paper is Gamow-Teller distributions.

### III. GAMOW-TELLER STRENGTH DISTRIBUTIONS

Our study focuses on the Gamow-Teller transitions from the lowest positive-parity states, which is natural for the most nuclei in the region above  $^{88}\text{Sr}$ , with the exception of the Y isotopes where the odd proton in the  $p_{1/2}$  shell is responsible for low-lying negative-parity states. Since our model space is not sufficient to reasonably reproduce negative-parity states in Sr isotopes where no valence protons are available, we do not calculate the transitions between these two isotope chains. Among the calculated nuclei, there are three cases where we chose the lowest experimental state to be the initial state for Gamow-Teller excitations rather than using our calculated lowest energy state. This affected two  $N = 51$  nuclei,  $^{92}\text{Nb}$  and  $^{94}\text{Tc}$ , where the calculation places  $2^+$  to be the lowest state, and the nucleus  $^{96}\text{Tc}$ .

The Gamow-Teller strength is calculated using the formula

$$GT_+ = \langle \sigma \tau \rangle^2 = \frac{1}{2J_i + 1} \sum_f \left| \langle \Psi_f | \left| \sum_k \sigma(k) \tau_+(k) \right| | \Psi_i \rangle \right|^2. \quad (1)$$

To obtain the strength distribution, we used the method of moments [18]. We performed 33 iterations for each  $J_f$  in all nuclei except for the decays of  $^{97}\text{Mo}$ , where we did 24 iterations per final state, and  $^{97}\text{Ag}$ , where a complete convergence was achieved. The  $GT_+$  strength inside the experimental  $Q_{\text{Ec}}$  window [19] is marked as  $B_{\text{Ec}}$ . This value is only an estimate, since we did not strive to achieve the convergence of states inside the  $Q$  window.

As previously discussed, our calculation overpredicts the Gamow-Teller strength; thus we include a hindrance factor,  $h$ , so that  $S(GT_+) = GT_+/h$ . This factor is found by comparing experimental data to the calculated Gamow-Teller total strength. For nuclei around  $^{100}\text{Sn}$ , the single-particle estimate of the Gamow-Teller strength is commonly used, since the main contribution comes from a transition of a  $g_{9/2}$  proton into a  $g_{7/2}$  neutron. The estimate is given by the following formula (see, e.g., [20]):

$$\Sigma GT_+ = \frac{N_{9/2}}{10} \left( 1 - \frac{N_{7/2}}{8} \right) GT_+(\text{}^{100}\text{Sn}), \quad (2)$$

where  $N_{9/2}$  is the occupation of the  $g_{9/2}$  shell by protons,  $N_{7/2}$  is the occupation of the  $g_{7/2}$  shell by neutrons in the initial state of a parent nucleus, and  $GT_+(\text{}^{100}\text{Sn}) = 17.78$  is the single-particle estimate of the total Gamow-Teller strength for  $^{100}\text{Sn}$ . In the simplest noninteracting shell model, the occupation numbers are replaced by the numbers of valence particles in the corresponding shells. This simplest estimate does not exactly reproduce our calculated strength even though the values are close. We illustrate this in Fig. 3, where the ratio of the Gamow-Teller strength obtained in the two models,  $GT_+/\Sigma GT_+$ , is plotted versus the ratio of protons in the  $g_{9/2}$  shell in these models. The latter ratio cannot drop below 1, because we do not include proton  $j$  shells above the  $g_{9/2}$  shell. However, correlations can increase the occupation of this shell, resulting in a  $GT_+/\Sigma GT_+$  ratio greater than 1. At the same time, neutron excitations into the  $g_{7/2}$  shell have the opposite effect, since the probability to enter this  $j$  shell during the Gamow-Teller transition decreases. There is no such blocking in the noninteracting model, since the number of neutrons is too small to start filling this shell. As can be seen from Fig. 3(a), the increase in the occupation of the  $g_{9/2}$  shell by protons is directly proportional to the increase in the shell-model Gamow-Teller strength. These additional proton excitations,  $\tilde{\pi}(g_{9/2}) \equiv \pi(g_{9/2}) - (Z_v - 2)$ , are affected by both the number of protons and the number of neutrons [see Fig. 3(b)]. If either of these two numbers increase, the proton excitations out of the  $p_{1/2}$  shell are reduced. The value of  $\tilde{\pi}(g_{9/2})$  is smaller if there already are more protons in the  $g_{9/2}$  shell. In addition, the increased number of neutrons reduces proton excitations because of a strong ( $\pi p_{1/2}, \nu d_{5/2}$ ) attraction in the residual interaction. The latter effect has to compete with a strong ( $\pi g_{9/2}, \nu g_{7/2}$ ) attraction, which increases the occupation of the  $\nu g_{7/2}$  shell as the number of protons increases

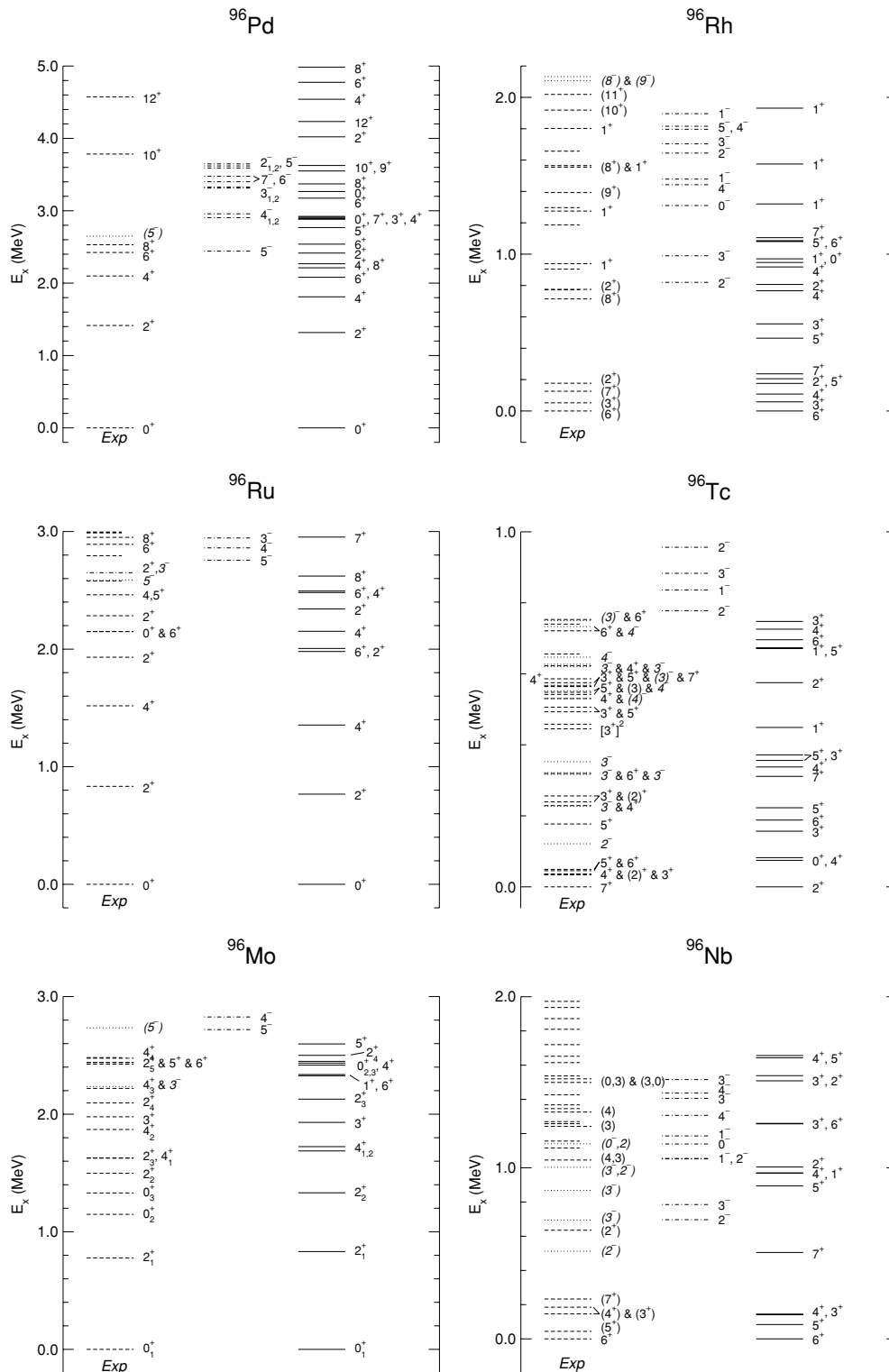


FIG. 1. Experimental [17] and calculated spectra in  $^{96}\text{Pd}$ ,  $^{96}\text{Rh}$ ,  $^{96}\text{Ru}$ ,  $^{96}\text{Tc}$ ,  $^{96}\text{Mo}$ , and  $^{96}\text{Nb}$ . Experimental levels are shown in the left column; the middle and right columns display calculated negative- and positive-parity states, respectively. Experimental positive-parity states are shown using dashed lines; negative-parity states are shown using dotted lines; states with known spin and uncertain parity are shown using dash-dotted lines; the states having both undetermined spin and parity are shown using a shorter dashed line. The sign “&” indicates that assignments refer to different experimental states, with the second one lying at a higher excitation energy. Since there is no spin ambiguity in the calculation, a comma is used in the middle and right columns in a similar situation. In some cases a subscript number is used to distinguish levels having the same spin and parity. At most, 10 calculated negative-parity states are shown for each nucleus. Only  $1^+$  calculated states are shown in  $^{96}\text{Rh}$  above  $E_x \approx 1.1$  MeV. Only negative-parity states and positive-parity states with  $J > 5$  are shown for  $^{96}\text{Ru}$  above  $E_x = 2.5$  MeV in the experimental spectrum. Experimental positive-parity states are cut off in  $^{96}\text{Mo}$  after  $E_x = 2.5$  MeV.

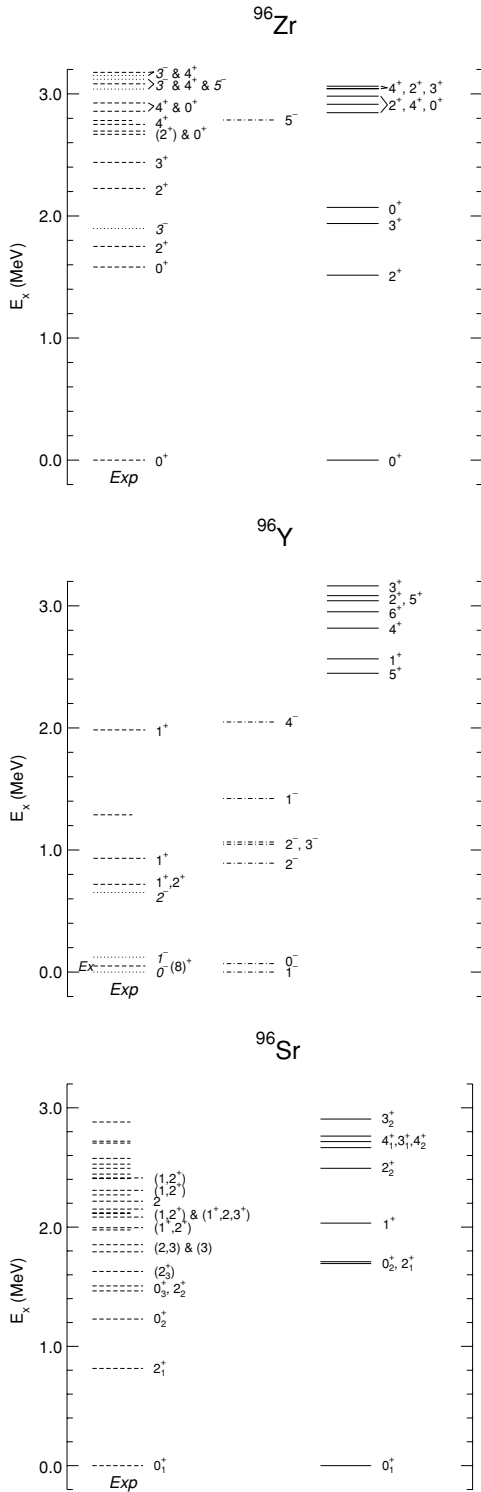


FIG. 2. Experimental and calculated spectra in  $^{96}\text{Zr}$ ,  $^{96}\text{Y}$ , and  $^{96}\text{Sr}$ . For notation, see caption of Fig. 1. The excitation energy of the isomeric state in  $^{96}\text{Y}$  with  $J^\pi = 8^+$  is not known [17].

[see Fig. 3(c)]. The increased blocking by the  $g_{7/2}$  neutrons results in decreasing shell-model Gamow-Teller strength along the isotope chain, as Fig. 3(a) shows. The figure also highlights that pairing effects influence the occupation of the  $\pi g_{9/2}$  and  $\nu g_{7/2}$  shells [see Fig. 3(b) and (c)]. The occupation of the  $g_{7/2}$

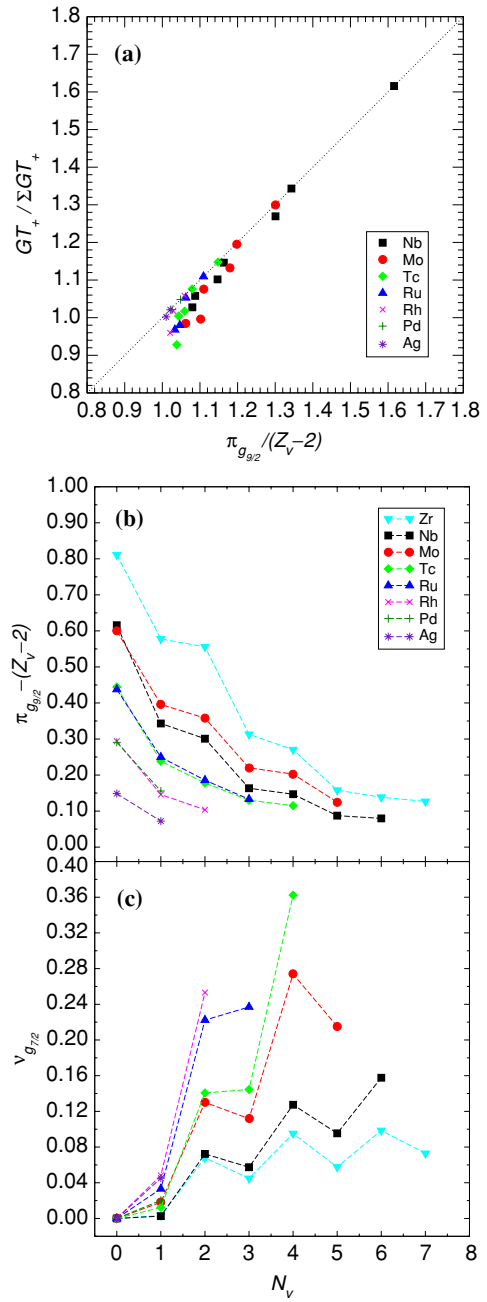


FIG. 3. (Color online) (a) The ratio of the total shell-model Gamow-Teller strength and the prediction from the noninteracting particle model plotted versus the ratio of the  $g_{9/2}$  proton number in these two models. (b) Isotopic dependence of the additional proton excitations into the  $g_{9/2}$  shell. (c) Isotopic dependence of the calculated number of neutrons in the  $g_{7/2}$  shell.

shell by neutrons as well as proton excitations out of the  $p_{1/2}$  shell gets smaller if the neutron number is odd. The value of  $\pi_{g_{9/2}}$  is affected by the number of empty time-reversed proton orbits. The odd proton in the  $g_{9/2}$  shell has a smaller effect on neutron excitations into the  $g_{7/2}$  shell than an addition of a proton, which makes even the number of the  $g_{9/2}$  protons in the noninteracting model.

Since our calculated total strength is reasonably close to the single-particle estimates, we could use the experimental hindrance factor quoted relative to the single-particle estimate:  $h^{\text{exp}} = GT_{\text{sp}}/GT_{\text{exp}}$ . Unfortunately, in this region, experimental information on  $h^{\text{exp}}$  is limited. Some of the calculated nuclei naturally decay from the ground state by  $\beta^-$  decay instead of electron capture, whereas in other nuclei, the  $Q$  window contains only a small fraction of the total strength. Thus the total  $GT_+$  strength could be obtained only by  $(n, p)$  or similar one-particle exchange reactions. An additional uncertainty in deriving the hindrance factor, even for nuclei where the  $Q$  window is large, comes from recent observations that  $\gamma$ -ray spectroscopy misses a significant fraction of the Gamow-Teller decay strength owing to sensitivity limits of detectors, a low population of nuclear levels close to the  $Q$  limit, and weak intensity of their decays [10,21]. This limitation can be overcome by combining a high-resolution  $\gamma$ -ray detector with total absorption spectrometry (TAS), as was done in a number of recent experiments on nuclei in the  $^{100}\text{Sn}$  region. For example, a study of  $^{97}\text{Ag}$  decay [11] showed that only 2/3 of the total Gamow-Teller strength is obtained by high-resolution  $\gamma$ -ray spectrometry, whereas the same number for  $^{102}\text{In}$  was about 1/8 [21].

One nucleus,  $^{97}\text{Ag}$ , has almost 98% of the total Gamow-Teller strength inside the  $Q_{\text{Ec}}$  window. We can use this nucleus to estimate the experimental hindrance factor. Hu *et al.* [11] reported  $\sum B(GT) = 3.00(40)$  based on TAS measurements, which leads to the hindrance factor  $h^{\text{exp}} = 4.24_{-0.50}^{+0.65}$ . Another nucleus where this window is large, and for which a TAS measurement is available, is  $^{98}\text{Ag}$  [22]. Hu *et al.* reported the total strength in  $^{98}\text{Ag}$  to be 2.7(4), giving the hindrance factor  $h^{\text{exp}} = 4.27_{-0.55}^{+0.74}$ , since the calculated  $B_{\text{Ec}}$  is 11.53 (which is 92% of the total Gamow-Teller strength inside the  $Q_{\text{Ec}} = 8.24$  MeV window). Thus the hindrance in two Ag isotopes,  $^{97}\text{Ag}$  and  $^{98}\text{Ag}$ , is of the order of 4.25, and we adopt this value for the total hindrance factor  $h$ . A similar value was used in Ref. [10]. We note that  $h$  consists of two factors,  $h = h_{\text{ga}}h_{\text{ms}}$ . The modification of  $g_A/g_V = 1$  in the nuclear medium yields an  $h_{\text{ga}} = 1.6$ , which implies that  $h_{\text{ms}} = 2.65$ . This value is commensurate with what one would obtain in highly truncated  $pf$ -shell calculations of the  $GT_+$  total strength relative to the full  $pf$  shell-model diagonalization values. We did not consider heavier nuclei for the hindrance estimate, because they are further away from our region of interest, and the possible  $Z$  dependence of this factor is not clear [11].

In this region, the only available total Gamow-Teller strength measured using the  $(n, p)$  reaction is for  $^{90}\text{Zr}$ . Raywood *et al.* [23] deduced a value of  $1.0 \pm 0.3$  for the total strength. Our calculated total strength for this isotope is  $S(GT_+) = 0.34$ , owing to the excitation of about 0.8 protons from the  $p_{1/2}$  to the  $g_{9/2}$  shell. We should note, however, that in our restricted model space there is only one  $1^+$  state in  $^{90}\text{Y}$ . These values can also be compared to recently reported measurements of  $3.0 \pm 1.9$  for the total strength by Sakai and Yako [24]. If, however, the noninteracting particle picture is assumed with only  $g_{9/2}$  protons contributing and no hindrance considered, then Eq. (2) would suggest 0.6 or 1.7 protons in the  $g_{9/2}$  shell for the two mentioned experiments, indicating that  $^{90}\text{Zr}$  is not a good closed-shell nucleus. Studies in

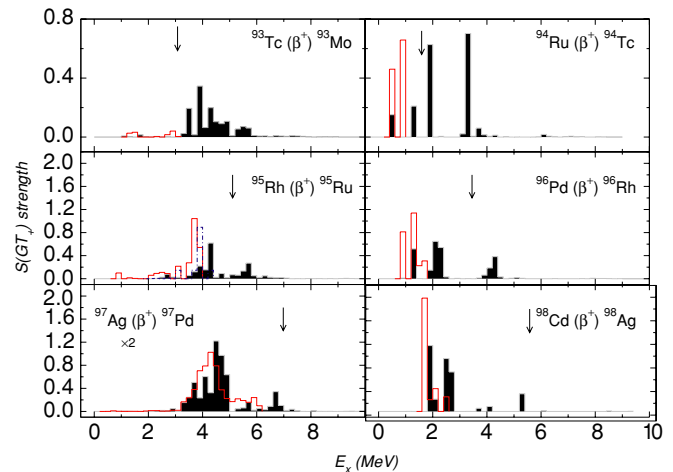


FIG. 4. (Color online) Gamow-Teller strength distributions from the ground states of  $N = 50$  isotones as a function of the excitation energy in the daughter nucleus. Two experimental sets are plotted for the decay of  $^{95}\text{Rh}$  (with values taken from [10,26]). The gray-shaded area is the calculated strength, the histogram represents the experiment. The experimental data suffer from detector sensitivity limits near the  $Q$  limit (indicated by an arrow), with the exception of  $^{97}\text{Ag}$ , where the data were obtained using TAS [11]. We show the strength in  $^{97}\text{Ag}$  scaled by a factor of 2. The bin size is 0.2 MeV.

Ref. [15] indicated that  $^{88}\text{Sr}$  is a preferable model-space core in comparison to  $^{90}\text{Zr}$ . The authors of Ref. [15] found that the addition of two valence protons outside of  $^{88}\text{Sr}$  actually served to stabilize the core in their calculations. In contrast, the discrepancy between our calculated Gamow-Teller strength and the experimental strength indicates that, for  $^{90}\text{Zr}$ , more channels should be open (i.e., the core should be broken) to obtain a larger Gamow-Teller strength. This situation is similar to calculations of the  $B(E2, 0^+ \leftarrow 2^+)$  in  $^{44}\text{Ti}$ , which requires breaking of the  $^{40}\text{Ca}$  core and allowing excitations from the  $sd$  to the  $pf$  shell to be properly described [25].

We turn now to strength distributions. Our calculated Gamow-Teller distributions in the decay of nuclear systems with a few valence protons, such as Zr or Mo isotopes, have the strength concentrated in a narrow energy range (less than 0.5 MeV) or sometimes in only one transition. The strength in systems with  $Z_v^p > 4$  (Tc and above) is distributed over the energy range of about 4 MeV. The Nb isotope chain is intermediate in this respect, because in the lowest configuration Nb has only one valence proton in the  $g_{9/2}$  shell, whereas decays to Zr isotopes are distributed over several states. We show these systematics using a few examples in the following.

In Figs. 4–6, we compare the calculated Gamow-Teller distributions with available data collected from several sources. All measurements were done in spontaneous decays. Data for  $N = 50$  and 51 isotones were obtained from Refs. [10,26,27]. The  $GT$  distribution in  $^{97}\text{Ag}$  [11] was obtained with a TAS measurement. We note that, in comparisons to experimental data, we do not include the sensitivity limits of experimental detectors. This sensitivity artificially cuts off the Gamow-Teller strength near the  $Q$  window so that calculated states are often not observed even 2 MeV below the  $Q$  window (see,

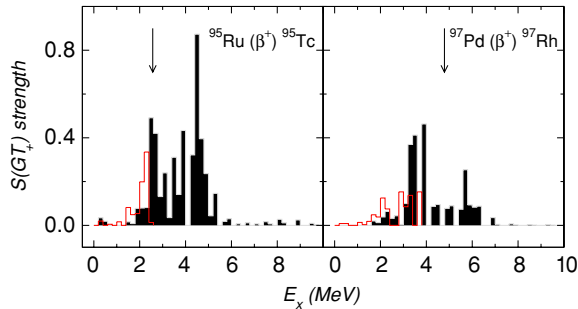


FIG. 5. (Color online) Gamow-Teller strength distributions from the ground states of two  $N = 51$  isotones:  $^{95}\text{Ru}$  and  $^{97}\text{Pd}$  (values taken from [27]). See also the caption of Fig. 4.

e.g., [10,11,21]). For this reason, comparisons to experiments are somewhat difficult to make, and one should focus on unambiguous regions of low-lying strength. In Table I we list fractions of the calculated Gamow-Teller strength that lie inside the  $Q$  window and compare them to the experimental values. The agreement with more recent experiments (the  $^{97,98}\text{Ag}$  nuclei) and heavier nuclei (where the  $Q$  window is larger) is better than in other cases. To evaluate whether the calculation underestimates the strength accessible in the  $\beta$ -decay experiments is difficult, because this question is directly related to the actual value of the hindrance factor. A comparison to the calculation by Brown and Rykaczewski [10] reveals some interaction dependence in the values. For example, they estimated  $f_{\text{Ec}} = 29\%$  and  $99\%$  in the decays of  $^{94}\text{Ru}$  and  $^{96}\text{Pd}$ , respectively, whereas our estimates are only  $19\%$  and  $72\%$ , respectively. Johnstone [26,27], following a different approach, estimated significantly higher fractions of the strength inside the  $Q$  window for most cases except  $^{95}\text{Ru}$ .

From Figs. 4–6 we note that the calculated strength distributions follow the trend observed in experiments. Most odd- $Z$   $N = 50$  isotones and  $N = 51$  isotones have little strength at low excitation energies ( $E_x \lesssim 2\text{--}3$  MeV), with the

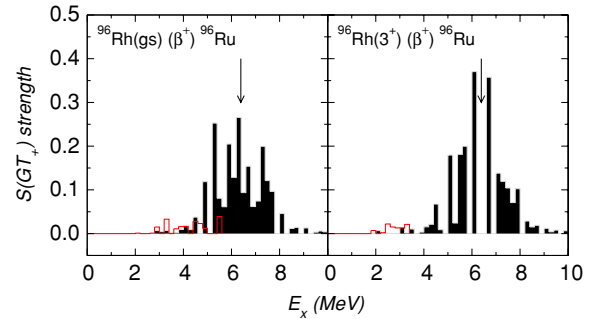


FIG. 6. (Color online) Gamow-Teller strength distributions from the ground state and the first excited state of  $^{96}\text{Rh}$  (values are taken from [27]). See also the caption of Fig. 4.

strength distributed among many states at a higher excitation energy, some of which are above the  $Q$  window. The strength in even-even nuclei, represented here by even- $Z$   $N = 50$  isotones, is concentrated in a few states.

The Gamow-Teller distribution in  $^{97}\text{Ag}$  shown in Fig. 4 is converged (around 60 iterations per  $J_f$  was required); thus the calculated shape is as good as it can be for the interaction. The centroid of the experimental Gamow-Teller strength distribution in  $^{97}\text{Ag}$  is lower than the calculation predicts:  $E_{\text{centr}}^{\text{exp}} = 4.3$  MeV versus  $E_{\text{centr}}^{\text{calc}} = 4.7$  MeV. This is one of the indicators that the interaction may require some fine-tuning.

We already showed and discussed parts of the calculated Gamow-Teller distributions in Figs. 4–6. Having in mind upcoming experiments [9] on Mo isotopes, we show the calculated distributions for the decays of Mo isotopes with masses  $A = 93\text{--}97$  in Fig. 7. The main contributions to the total strength are located within a 1-MeV energy range around the centroid. The decays of Tc isotopes (see Fig. 8) have the strength distributed within a 4-MeV range. These two isotope chains display the difference in the decays of even-even and odd-odd nuclei that we already discussed.

TABLE I. Fraction of the calculated Gamow-Teller strength inside the  $Q_{\text{Ec}}$  window,  $f_{\text{Ec}} = B_{\text{Ec}}/GT_+$ , and experimental  $\Sigma B(GT)$  strength.

Parent nucleus	$GT_+$	$B_{\text{Ec}}$	$f_{\text{Ec}}$ %	$B_{\text{Ec}}/h$	$\Sigma B(GT)$	Ref.
$^{93}\text{Tc}$	6.12	0.13	2	0.03	0.13	[26]
$^{94}\text{Tc}$	5.74	0.13	2	0.03	—	
$^{94}\text{Ru}$	7.89	1.53	19	0.36	1.0	[10]
$^{95}\text{Tc}$	5.43	0.08	1	0.02	—	
$^{95}\text{Ru}$	7.49	0.59	8	0.14	0.8	[27]
$^{95}\text{Rh}$	9.41	6.35	67	1.49	1.3, 2.5	[26]
$^{96}\text{Tc}$	5.36	0.04	1	0.01	—	
$^{96}\text{Rh}$	9.05	5.14	57	1.21	0.2	[27]
$^{96}\text{Pd}$	11.18	8.08	72	1.90	2.4	[10]
$^{97}\text{Rh}$	8.53	2.60	30	0.61	—	
$^{97}\text{Pd}$	10.90	7.38	68	1.74	0.9	[27]
$^{97}\text{Ag}$	12.71	12.49	98	2.34	3.0	[11]
$^{98}\text{Ag}$	12.47	11.53	92	2.71	2.7	[22]
$^{98}\text{Cd}$	14.48	14.40	99	3.39	3.5	[26]

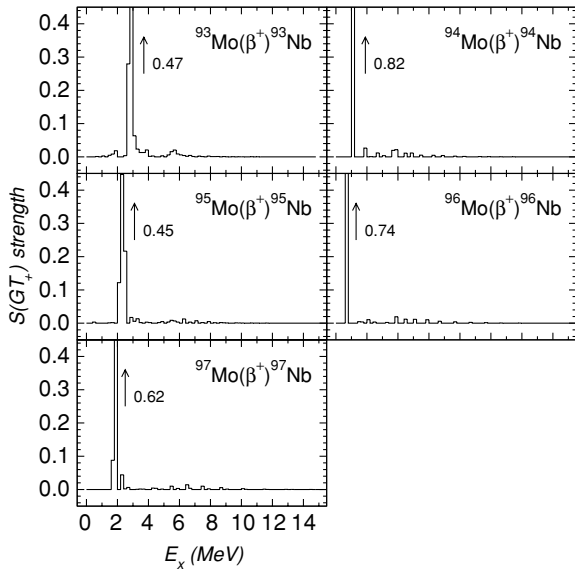


FIG. 7. Calculated Gamow-Teller distributions in Mo isotopes with masses  $A = 93-97$  ( $N = 50-55$ ). The arrow indicates that the value inside the bin (shown by a number beside it) is greater than the upper limit of the y axis. The bin size is 0.2 MeV.

We also show the distributions for Nb isotopes (see Fig. 9). There we observe the strength migration from higher energies to lower energies as the neutron number increases. Simultaneously, the Gamow-Teller distribution gets narrower, until the entire strength is gathered in one transition.

We turn now to a discussion of the calculated total Gamow-Teller strength and the centroids. The isotopic dependence of the total strength is smooth with the strength decreasing together with the increasing number of neutrons and/or the decreasing number of valence protons in the  $g_{9/2}$  shell [see the discussion after Eq. (2)]. Assuming no mass dependence, we can derive an approximate formula:  $GT_+ = 0.086(Z_v - 1.5)(20 - N_v)$ . [The factor  $(20 - N_v)$  is due to the relative unimportance of the  $h_{11/2}$  shell because of its negative parity.] This form is somewhat similar to the dependence  $Z_v(20 - N_v)/A$  observed in the  $pf$ -shell nuclei (see, e.g., [28]). The difference may be related to the active  $j$  shells. In the

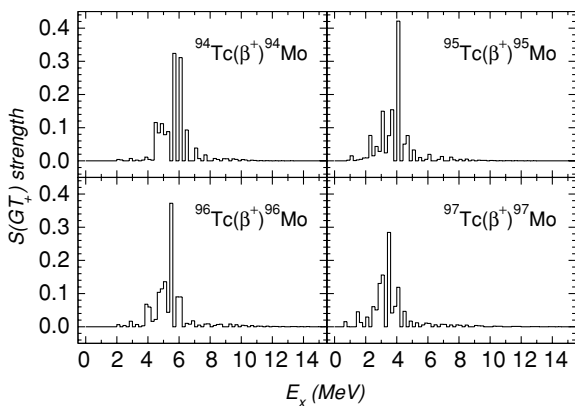


FIG. 8. Calculated Gamow-Teller distributions in Tc isotopes with masses  $A = 94-97$ . See also the caption to Fig. 7.

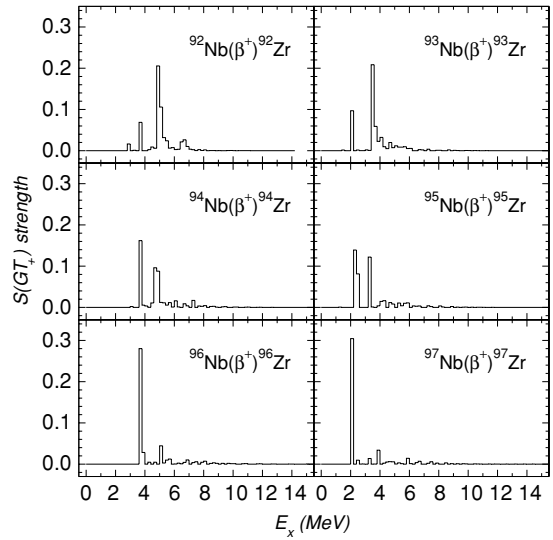


FIG. 9. Calculated Gamow-Teller distributions in Nb isotopes with masses  $A = 92-96$ . See also the caption to Fig. 7.

$pf$ -shell nuclei, discussed in Ref. [28], protons predominantly occupy the  $f_{7/2}$  shell; thus its occupation is proportional to the number of valence protons. In contrast, in our model space, the occupancy of the  $g_{9/2}$  proton shell increases due to excitations out of the  $p_{1/2}$  shell via configuration mixing. This increase is greater for isotopes closer to the core nucleus (around 0.6) and is 0.2 for  $A = 97$  nuclei with  $Z_v > 2$ . The formula's  $\chi^2$  per degree of freedom is 0.05.

Another systematic relates to the centroids of the  $GT_+$  distribution. If plotted with respect to the lowest positive-parity state of the daughter nucleus, the centroids of Gamow-Teller distributions show a characteristic odd-even staggering (see Fig. 10). They are low in even-even nuclei, high in odd-odd

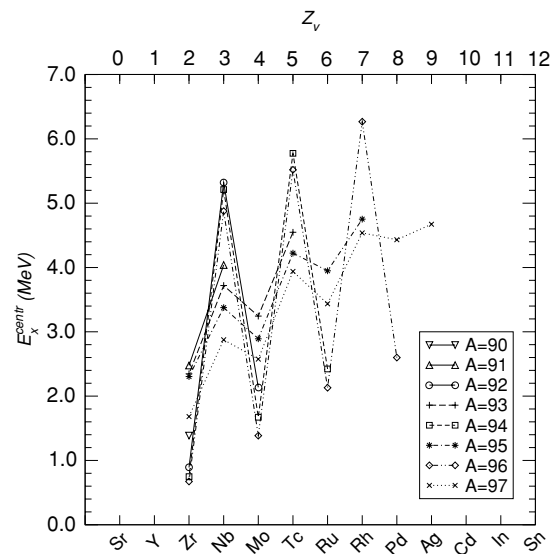


FIG. 10. Excitation energy of the centroid in the calculated nuclei. For  $Zr \xrightarrow{\beta^+} Y$  decay, the excitation energy was calculated from the lowest positive-parity state in Y.

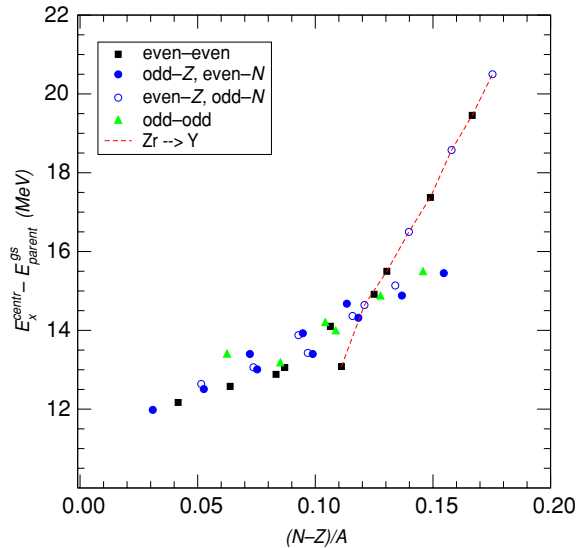


FIG. 11. (Color online) Energy of the  $GT_+$  centroid with respect to the calculated ground-state energy of the parent nucleus as a function of  $(N - Z)/A$ .

nuclei, and average in odd- $A$  nuclei. A similar trend was observed in the mid- $pf$ -shell nuclei [29].

Langanke and Martínez-Pinedo [5] interpreted this odd-even staggering as a result of pairing energy contributions to the mass splitting between the parent and daughter nuclei (see also [30]). The pairing structure effect goes away if the centroids are measured with respect to the parent nucleus. We plotted the centroid energies calculated in this way in Fig. 11. We also included the Coulomb energy difference, calculated using the formula [31]  $E_c = 0.72(Z^2/A^{1/3})(1 - 1.69/A^{2/3})$ , but ignored the proton-neutron mass difference and the splitting between the proton and neutron single-particle orbits, which would be present if the lowest single-particle energies would be taken with respect to the core nucleus,  $^{88}\text{Sr}$ . The figure shows that centroid energies indeed lose information about the pairing structure. It is interesting to note that there seems to be a crossover behavior, which we highlighted by connecting the points corresponding to the decays of Zr isotopes. These centroid energies follow a linear dependence as well, but the inclination is different from that in other nuclei. This behavior is probably related to the fact that  $GT_+$  strength in Zr isotopes is due to the proton excitations out of the  $p_{1/2}$  shell.

#### IV. DISTRIBUTED-MEMORY SHELL-MODEL CODE

Our calculations were performed using a new parallel shell-model code ORPAH (Oak Ridge parallel shell model code), which is still under development. The basic ideas are similar to those employed in the serial  $m$ -scheme computer code ANTOINE [32,33]. However, there are differences in the approach, since the code was developed by targeting the distributed-memory computational paradigm. Although the distributed-memory approach sets no limits on the available memory or the number of processors involved in the computation, a natural limitation occurs because of the need to

communicate data from one processor to another, a process that for collective operations scales as  $N_p^2$ , where  $N_p$  is the number of processors. However, even in cases when communication becomes unfavorable, there is still a possible trade-off because of a greater amount of available memory.

The most time-consuming part of the shell-model problem is the operation of the Hamiltonian on a vector,  $H\Psi$ , producing a new vector. Long computation time demands a good load-balancing at this step, since each processor should be assigned a similar amount of work for an effective use of computational resources. One Lanczos iteration consists of two substeps: a production of a new vector and its subsequent reorthogonalization to previous ones. We parallelize each substep in a different way. First, to speed up vector-vector operations we assign a fixed, approximately equal number of the basis vectors to each processor. Owing to the orthogonality of the basis states, the amplitudes are independent, and vector-vector operations can be performed on each processor in parallel with a collective addition of the partial results to obtain values of the scalar products. This distribution of amplitudes creates the need to send them to other processors when a new vector is created during the  $H\Psi$  operation. Second, for a time-efficient parallel  $H\Psi$  operation the amplitudes are grouped into smaller portions, as we discuss in the following. Each processor works on a set of pairs of these groups, which are assigned in a time-balanced way before the Lanczos iterations start. The goal is that each processor would spend an approximately equal amount of time producing pieces of the final vector. These pieces are then sent to the appropriate processors after each iteration, where they are added up. When all pieces are collected, the second substep of Lanczos procedure, reorthogonalization, starts.

In the following we give some more details of the code. Similar to ANTOINE, the code numerically builds “blocks” of identical-particle Slater determinants having the same quantum numbers and sets up tables allowing construction of the elements of the Hamiltonian matrix [33]. Differences arise from the need to split blocks for a more efficient computation. If the model space dimension is  $D$ , and there are  $N_p$  processors, then the part of amplitudes that reside on a particular processor has size  $D/N_p$ . For a sufficiently large number of processors,  $D/N_p$  can get smaller than the size of the largest block  $s_l$ . (In general, the original blocks have greatly varying sizes.) This would limit the maximum reasonable number of processors, because additional processors would keep track of only a small amount of amplitudes. An additional limitation would come from the  $H\Psi$  computation. Operations involving this largest block are also the most time-consuming, since for a dense matrix the number of matrix-vector operations scales like  $s_l^2$ , whereas the sparsity affects all groups. To avoid these limitations we decided to split the blocks, which also allows a better work balance of the  $H\Psi$  operation. If  $g_i$  is a group of initial amplitudes, then the operation with a complete Hamiltonian produces amplitudes  $(Hg_i)$  belonging to several final groups  $g_f$ . Smaller groups take less computation time and allow a better-balanced assignment of tasks  $(g_i, g_j): (g_i^{\text{ini}}, g_j^{\text{ini}}) \rightarrow (g_i^{\text{fin}}, g_j^{\text{fin}})$ , where  $g_i^{\text{fin}} (g_j^{\text{fin}})$  is a part of  $Hg_j^{\text{ini}} (Hg_i^{\text{ini}})$  amplitudes belonging to the amplitude group  $g_i (g_j)$ .

During the operation of the Hamiltonian acting on a vector, the amplitudes are requested from other processors as needed, according to the assigned task list. Some of the amplitudes are buffered in the processor's memory, allowing the processor to compute while simultaneously waiting for additional amplitudes to arrive. To make this possible each processor runs one computation and one communication thread. Having calculated the assigned contributions to the final Lanczos vector, the processor sends those amplitudes to the appropriate processor, where they are added up. The final Lanczos vector is reorthogonalized to previous vectors. Because of the orthogonality of the basis, each processor can produce a partial sum of the scalar product, and (global) communication is needed only to obtain the total sum. When the vector overlaps are available, the final orthogonal vector is produced and is stored on processors by the assigned pieces.

There is no coded-in restriction on the number of processors, with the exception that the minimum number of processors is two, because of the manager-worker algorithm employed in the Hamiltonian table setup procedure. The current version of the code can calculate eigenvalues and eigenvectors of the Hamiltonian, the total angular momentum and isospin, as well as  $GT_{\pm}$  properties. Some computations were done on a 2–4 CPU computer running Linux; others were done at the NERSC computer Seaborg using up to 80 processors. To test the limitations of the code, we tried different problems. The largest dimension that we were able to solve was the ground-state energy of  $^{52}\text{Fe}$  ( $D = 110 \times 10^6$ ) on 48 processors. The current setup did not allow us to reach such dimensions in the region of our study, where proton and neutron spaces are very asymmetric.

The performance of a parallel code is usually assessed by plotting the speed-up time as a number of processors. The need to deliver amplitudes as well as summation of partial overlaps creates a communication overhead on top of the time needed to produce the final Lanczos vector. The latter operation is well balanced (i.e., is inversely proportional to the number of processors), whereas the overhead depends on the number of processors involved in the calculation. Theoretically, this time is proportional to the number of processors squared. However, we were unable to obtain a consistent value of the time per iteration within one multiprocessor run, and so we delay the speed-up evaluation until further improvement in the code performance. In spite of this difficulty, we consider the distributed-memory computation to be a promising venue to solve large-scale shell-model problems.

## V. SUMMARY

We calculated nuclei above  $^{88}\text{Sr}$  having masses  $A = 90$ – $97$  using a realistic effective interaction derived from the CD-Bonn potential. The agreement between the calculated and measured spectra is satisfactory. Improvements to the interaction through fine-tuning of the matrix elements could be useful to obtain the finer spectroscopic details, including the level ordering or the placement of negative-parity states in several nuclei, but this is beyond the scope of this exploratory

work, which focuses on the Gamow-Teller properties in the selected region of nuclei.

We also calculated the total Gamow-Teller strength and strength distributions for the decays in the electron-capture direction. We found that the total strength follows the single-particle estimate based on the  $\pi g_{9/2}$  and  $\nu g_{7/2}$  occupation numbers obtained from the ground-state wave functions of the parent nucleus, although the values differ slightly from a naive single-particle shell-model picture. Calculated strength distributions appear to reasonably recover experimental distributions in regions that are unaffected by detector sensitivity limits. From TAS data on  $^{97}\text{Ag}$ , we were able to obtain an estimate of the phenomenological quenching factor relative to single-particle estimates. Furthermore, our Gamow-Teller distribution for  $^{97}\text{Ag}$  reproduces the measured data (see Fig. 4). By analyzing the centroids of the Gamow-Teller distributions, we found that the odd-even staggering behavior disappears if the centroids are measured from the parent ground state, as was suggested by Langanke and Martínez-Pinedo [5]. We also observed that the centroids measured in this way have a quasilinear dependency on the parametrization  $(N - Z)/A$ , with a different inclination for nuclei where no protons are present in the  $g_{9/2}$  shell in the noninteracting picture. Finally, we made several predictions of the strength distributions for the measurements that may soon be available in mass  $A = 92$ – $97$  nuclei. To resolve the question of the Gamow-Teller strength quenching in this region both the updated experimental information as well as improved  $0\hbar\omega$  theoretical calculations are required.

The description of low-lying Gamow-Teller strength distributions in a large range of nuclei (from roughly mass  $A = 50$  to mass  $A = 150$ ) is one important ingredient in understanding type II supernova explosions, since electrons get captured by nuclei through these levels. Of course, this is not the whole story since first- and second-forbidden transitions (which are typically difficult to access in the laboratory) also play an important role in the cross-section and rate calculations relevant for supernovae. For low-energy capture, the Gamow-Teller transitions will dominate. They also dominate the neutrino-nucleus scattering that may occur at later times in the supernova event. Theoretical calculations can provide rate estimates for these processes. However, measurements are necessary to validate the estimates. Additional experimental data for the nuclear region discussed in this paper are required to put constraints on the theoretical predictions and to help improve them.

## ACKNOWLEDGMENTS

We are pleased to acknowledge useful discussions with T. Engeland, M. Hjorth-Jensen, K. Langanke, K. Rykaczewski, R. G. T. Zegers, G. Martínez-Pinedo, B. A. Brown, and I. P. Johnstone. We are also grateful to M. Karny and L. Batist for providing us TAS data on  $^{97}\text{Ag}$ . Oak Ridge National Laboratory (ORNL) is managed by UT-Battelle, LLC, for the U.S. Department of Energy under Contract No. DE-AC05-00OR22725. The work of A. J. was partially supported by the Department of Energy through the Scientific Discovery through Advanced Computing (SciDAC) program.

- [1] B. A. Brown and B. H. Wildenthal, *Annu. Rev. Nucl. Part. Sci.* **38**, 29 (1988).
- [2] K. Langanke, D. J. Dean, P. B. Radha, Y. Alhassid, and S. E. Koonin, *Phys. Rev. C* **52**, 718 (1995).
- [3] E. Caurier, K. Langanke, G. Martínez-Pinedo, and F. Nowacki, *Nucl. Phys.* **A653**, 439 (1999).
- [4] G. Martínez-Pinedo, A. Poves, E. Caurier, and A. P. Zuker, *Phys. Rev. C* **53**, 2602(R) (1996).
- [5] K. Langanke and G. Martínez-Pinedo, *Nucl. Phys.* **A673**, 481 (2000).
- [6] K. Langanke, G. Martínez-Pinedo, J. M. Sampaio, D. J. Dean, W. R. Hix, O. E. B. Messer, A. Mezzacappa, M. Liebendörfer, H.-T. Janka, and M. Rampp, *Phys. Rev. Lett.* **90**, 241102 (2003).
- [7] W. R. Hix, O. E. B. Messer, A. Mezzacappa, M. Liebendörfer, J. Sampaio, K. Langanke, D. J. Dean, and G. Martínez-Pinedo, *Phys. Rev. Lett.* **91**, 201102 (2003).
- [8] R. G. T. Zegers *et al.*, *Nucl. Phys.* **A731**, 121(c) (2004).
- [9] R. G. T. Zegers (private communication).
- [10] B. A. Brown and K. Rykaczewski, *Phys. Rev. C* **50**, 2270(R) (1994).
- [11] Z. Hu *et al.*, *Phys. Rev. C* **60**, 024315 (1999).
- [12] M. Lipoglavšek *et al.*, *Phys. Rev. C* **65**, 021302(R) (2002).
- [13] R. Machleidt, F. Sammarruca, and Y. Song, *Phys. Rev. C* **53**, 1483(R) (1996).
- [14] M. Hjorth-Jensen, T. T. S. Kuo, and E. Osnes, *Phys. Rep.* **261**, 125 (1995).
- [15] A. Holt, T. Engeland, M. Hjorth-Jensen, and E. Osnes, *Phys. Rev. C* **61**, 064318 (2000).
- [16] Retrieved from Nucl. Data Sheets on-line, <http://ie.lbl.gov/ensdf/welcome.htm>, on June 15, 2004.
- [17] L. K. Peker, *Nucl. Data Sheets* **68**, 165 (1993).
- [18] R. R. Whitehead, in *Moment Methods in Many Fermion Systems*, edited by B. J. Dalton *et al.* (Plenum, New York, 1980).
- [19] G. Audi, A. H. Wapstra, and C. Thibault, *Nucl. Phys.* **A729**, 337 (2003).
- [20] I. S. Towner, *Nucl. Phys.* **A444**, 402 (1985).
- [21] M. Gierlik *et al.*, *Nucl. Phys.* **A724**, 313 (2003).
- [22] Z. Hu *et al.*, *Phys. Rev. C* **62**, 064315 (2000).
- [23] K. J. Raywood *et al.*, *Phys. Rev. C* **41**, 2836 (1990).
- [24] H. Sakai and K. Yako, *Nucl. Phys.* **A731**, 94(c) (2004).
- [25] D. J. Dean, M. T. Ressel, M. Hjorth-Jensen, S. E. Koonin, K. Langanke, and A. P. Zuker, *Phys. Rev. C* **59**, 2474 (1999).
- [26] I. P. Johnstone, *Phys. Rev. C* **44**, 1476 (1991).
- [27] I. P. Johnstone, *Phys. Rev. C* **57**, 994 (1998).
- [28] S. E. Koonin, D. J. Dean, and K. Langanke, *Phys. Rep.* **278**, 1 (1997).
- [29] S. E. Koonin and K. Langanke, *Phys. Lett.* **B326**, 5 (1994).
- [30] F. K. Sutaria and A. Ray, *Phys. Rev. C* **52**, 3460 (1995).
- [31] W. D. Myers and W. J. Swiatecki, *Nucl. Phys.* **81**, 1 (1966).
- [32] E. Caurier, computer code ANTOINE, IReS, Strasbourg, 1989.
- [33] E. Caurier, G. Martínez-Pinedo, F. Nowacki, A. Poves, J. Retamosa, and A. P. Zuker, *Phys. Rev. C* **59**, 2033 (1999).